Photo-Induced Reactions of Nitrate in Aqueous Microdroplets by Triplet Energy Transfer

Pyeongeun Kim, Christian Boothby, Vicki H. Grassian, Robert E. Continetti**

Department of Chemistry and Biochemistry, University of California San Diego, 9500 Gilman Drive, La Jolla, California, 92093-0340, United States

Corresponding Authors

*Vicki H. Grassian − Department of Chemistry and Biochemistry, University of California San Diego, 9500 Gilman Drive, La Jolla, California, 92093-0340, USA. E-mail: vhgrassian@ucsd.edu

*Robert E. Continetti - Department of Chemistry and Biochemistry, University of California San Diego, 9500 Gilman Drive, La Jolla, California, 92093-0340, USA. E-mail: rcontinetti@ucsd.edu

ABSTRACT

In-situ Raman spectroscopy of single levitated aqueous microdroplets irradiated by dual-beam (266 and 532 nm) lasers demonstrates that nitrate anion (NO_3^-) can be depleted in the droplet through an energy transfer mechanism following excitation of sulfanilic acid (SA), a UV-absorbing aromatic organic compound. Upon 266 nm irradiation, fast decrease of NO_3^- concentration was observed when SA is present in the droplet. This photo-induced reaction occurs

without the direct photolysis of NO_3^-. Instead, the rate of NO_3^- depletion was found to be dependent on the initial concentration of SA and pH of the droplet. Based on absorption-emission spectral analysis and excited-state energy calculations, triplet-triplet energy transfer between SA and NO_3^- is proposed as the underlying mechanism for the depletion of NO_3^- in aqueous microdroplets. These results suggest that energy transfer mechanisms initiated by light-absorbing organic molecules may play a significant role in NO_3^- photochemistry.

TOC GRAPHICS

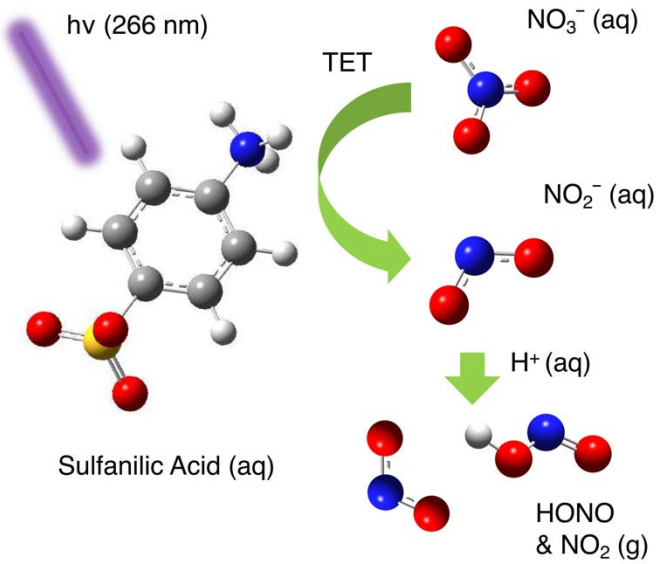

KEYWORDS

Aerosols, Raman spectroscopy, Nitrate, Photochemistry, Triplet Energy Transfer, Electrodynamic Balance, HONO

Aerosols are ubiquitous in nature, and greatly impact the Earth's climate and human health.[1–4] In the atmosphere, aerosols can undergo various chemical reactions including heterogeneous reactions, photochemical reactions by irradiation of ultraviolet (UV) light, and accelerated reactions of organic molecules.[5–9] In particular, photochemical reactions of aqueous NO_3^- are of great interest in terms of atmospheric relevance because the reactions produce highly reactive species such as NO_2, HONO, and hydroxyl radical (·OH).[10] NO_3^- is a common contaminant found in surface waters and atmospheric aerosols due to agricultural activity.[11,12] Since the photolysis of NO_3^- by UV-absorption can play a role in modulating the concentration of volatile organic compounds and affect the formation of secondary organic aerosols (SOAs), unraveling the pathways and rates of photochemical reactions is an essential step for gaining a quantitative understanding of the chemical evolution of atmospheric aerosols containing NO_3^-.[13–21]

The UV-absorption spectrum of aqueous NO_3^- contains a very weak n → π* band centered near 302 nm and a strong π → π* band at 200 nm.[22] The n → π* transition of NO_3^- is forbidden by symmetry for the two electronic states involved. However, the influence of solvent molecules breaks the symmetry, relaxing the dipole-forbidden character of the transition and leading to a weak absorption band in the 280 – 330 nm range.[23,24] This transition of NO_3^- is widely studied as the band overlaps the solar UV spectrum. The direct photolysis of aqueous NO_3^- at this wavelength range leads to two main dissociation pathways.[22]

$$NO_3^- \xrightarrow{h\nu} NO_2^- + O(^3P) \qquad \Phi = 1.1 * 10^{-3} \qquad (1)$$

$$NO_3^- \xrightarrow{h\nu} NO_2\,(g) + \cdot O^- \qquad \Phi = 9.2 * 10^{-3} \qquad (2a)$$

$$\cdot O^- + H_2O \rightarrow \cdot OH + OH^- \qquad (2b)$$

In acidic conditions, the nitrite anion (NO_2^-) can readily protonate and produce gaseous HONO.[25]

$$NO_2^- + H_3O^+ \rightarrow H_2O + HONO\,(g) \qquad (3)$$

HONO is a major precursor of ·OH radicals that play a key role as one of the most important oxidants in the atmosphere.[14] However, field studies have reported unexpectedly high emissions of HONO during the day,[26,27] and it has been suggested that UV-photolysis of NO_3^- is potentially an important unaccounted source for high daytime HONO production.[28]

Recent studies have revealed that dissolved organic matter which absorbs UV light can act as a photosensitizer and enhance the photolysis of NO_3^-.[29–31] Wang *et al.* showed an increased quantum yield of NO_2^- from photolysis of NO_3^- in the presence of UV-absorbing vanillic acid.[29] Gen *et al.* used iron-organic complexes to measure increased HONO production rates.[30] The photosensitizing effect of marine chromophoric dissolved organic matter (m-CDOM) was compared with other organic photosensitizers (humic acid and 4-benzoylbenzoic acid) by Mora-Garcia *et al*.[31] Even more recently, Jiang et al. reported that excited state NO_2 can enhance the formation of HONO in the presence of NO_3^- and humic-like substances.[32] These studies suggested that the presence of photosensitizers increases the production rates of HONO, however, the exact mechanisms of photosensitized reactions of NO_3^- leading to the enhanced production of HONO remain unclear. Those studies made use of a Xe lamp with a broadband output between 290 – 350 nm as a source of UV radiation, simultaneously promoting photosensitized reactions and direct photolysis of NO_3^-.[29–31] This choice of light source makes it difficult to isolate and quantify the effect of photosensitizers alone, as the rate of depletion of NO_3^- has contributions from both photosensitized reactions and direct photolysis of NO_3^-. Therefore, there is a great demand for an investigation that separates the photosensitized reaction of NO_3^- from direct photolysis to provide a better understanding of the factors governing enhanced HONO and NO_2 production in organic-laden aqueous aerosols.

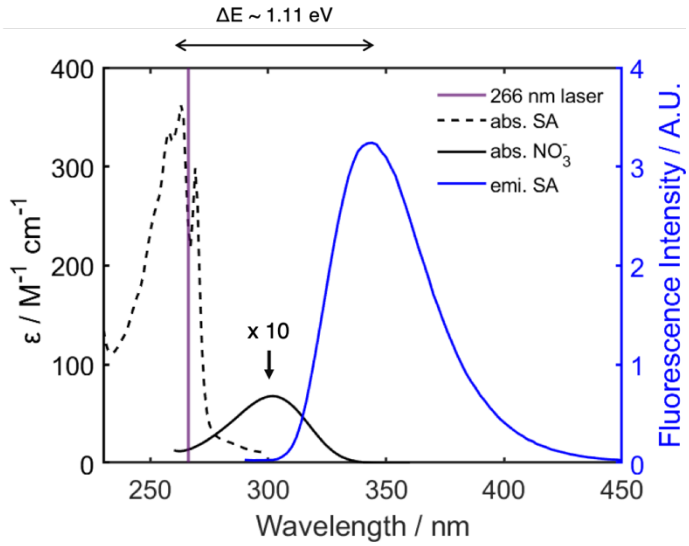

Figure 1. Absorption-emission spectra of SA and NO_3^-. Left y-axis represents the molar extinction coefficient (ε, units: M^{-1} cm^{-1}) of SA and NO_3^-. The $S_0 \rightarrow S_1$ absorption band of SA is located at 230 – 280 nm range (dashed black line). ε of NO_3^- is magnified by 10 times (solid black line) because of its relatively small value compared to SA. y-axis on the right side shows emission intensity in arbitrary units. The emission band from SA is observed at 300 – 450 nm (solid blue line) with peak position near 350 nm. The energy difference between absorption and emission peaks of SA is about 1.11 eV.

To effectively simulate photo-induced reactions in atmospheric aerosols, an environment-controlled electrodynamic balance (EDB) was utilized for the levitation of single aqueous microdroplets.[33,34] Sample solutions for droplet generation were made up with water, sodium nitrate ($NaNO_3$), citric acid (CA), and sulfanilic acid (SA), and the pH of the droplets was adjusted using a citric acid/sodium citrate buffer. SA was chosen as a model light-absorbing organic molecule, and the 266 nm output from a Nd:YAG laser was used as a source of photoexcitation to

effectively separate photosensitized reactions from direct photolysis of NO_3^-. **Figure 1** shows the absorption and emission spectra of SA (pH = 0.82) in bulk solution along with the absorption spectrum of aqueous $NaNO_3$ in bulk solution scaled up by a factor of 10. SA has a strong UV-absorption band at 230 – 280 nm,[35] thus it is effectively excited by the 266 nm laser irradiation ($\varepsilon > 200\ M^{-1}\ cm^{-1}$). Photolysis of NO_3^- by 266 nm is improbable due to its low molar extinction coefficient ($\varepsilon = 1.5\ M^{-1}\ cm^{-1}$) at this wavelength.[13] Emission of SA was observed in the 300 -450 nm range. The relationship between the electronic structure of SA and reactions of NO_3^- is explained in later paragraphs.

Figure 2A shows a simplified schematic of the EDB and a levitated microdroplet. The 266 nm irradiation photoexcites the SA in the droplet, while the 532 nm laser produces *in situ* Raman spectra and Mie scattering images for tracking the size of the particle. Real-time molality, m, (mol kg^{-1}) of NO_3^- ($[NO_3^-]$) of the levitated microdroplets were measured by quantifying the intensity of the characteristic Raman peak for the NO_3^- symmetric stretch ($\nu_s(NO_3^-)$, 1050 cm^{-1}) relative to the C-H stretch (ν(C-H), 2950 cm^{-1}) in CA (**Figure 2B**). Details of the determination of $[NO_3^-]$ using a calibration curve are given in the supplementary information (SI **Figure S1**). The diameter of the droplets over the course of the measurement were measured using Mie scattering imaging (MSI, **Figure S2**). As the levitated microdroplets with pH ~ 0.5 were irradiated by 266 nm, a decrease in $[NO_3^-]$ in the presence of SA was observed over ~30-minute reaction timeframe. Observations were limited to ~30 minutes of 266 nm irradiation, as individual droplets became unstable and eventually were ejected from the EDB. A possible reason for this limitation is discussed later.

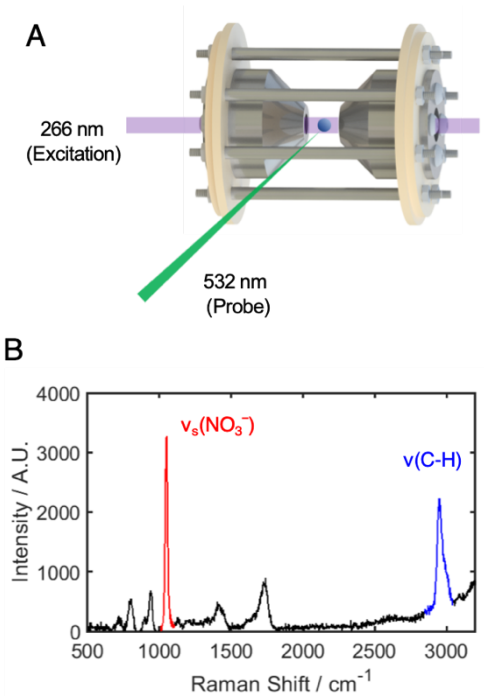

Figure 2. (A) Schematic of the EDB with a levitated aqueous microdroplet. In these experiments, an aqueous droplet with 80-100 µm diameter, is trapped between the two endcap electrodes of the EDB. A 266 nm beam (purple) is passed through two small holes of the endcap electrodes. The beam waist of the 266 nm laser and size of the droplet are exaggerated for visibility. A 532 nm (green) probe beam is focused on the droplet perpendicular to the 266 nm beam. (B) The sample Raman spectrum of a droplet generated from an aqueous solution of CA, SA and $NaNO_3$. The $\nu_s(NO_3^-)$ peak at 1050 cm^{-1} and ν(C-H) peak of SA at 2950 cm^{-1} are colored red and blue, respectively.

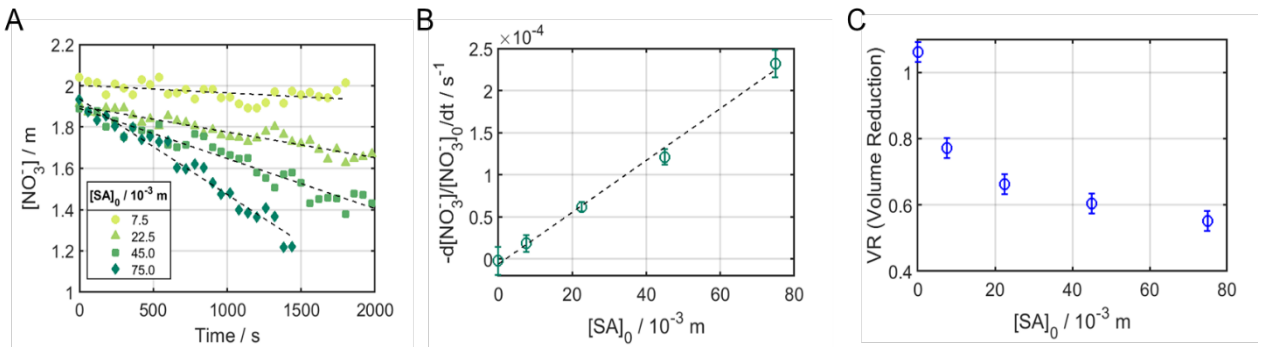

Figure 3. Photo-induced depletion of NO_3^- from the levitated aqueous microdroplets. (A) Measured [NO_3^-] as a function of irradiation time with varying $[SA]_0$ in the range up to 75.0 x 10^{-3} m. Dashed black lines represent linear fits to the data. Data with $[SA]_0 = 0$ showed no NO_3^- depletion and is not pictured here for clarity, instead the data are provided in the SI (**Figure S4**). (B) Relative photo-induced rates (s^{-1}) of NO_3^- depletion versus initial [SA]. Error bars represent 95% confidence intervals of the linear fit of [NO_3^-] versus time. Dashed line shows linear relationship between depletion rate of NO_3^- and $[SA]_0$. (C) Volume reduction (VR) of the irradiated droplets versus $[SA]_0$. Error bars represent uncertainties from the approximated refractive index values for the droplets.

Figure 3A shows the depletion of [NO_3^-] as a function of 266 nm irradiation time with varying initial concentrations of SA ($[SA]_0$). The loss of NO_3^- is due to the reduction of NO_3^- into HONO (g) and NO_2 (g) which are volatile and can partition from the droplet.[31,36] The effect of excited-state SA as a reaction initiator for reduction of NO_3^- is apparent as higher $[SA]_0$ leads to faster depletion of NO_3^-. **Figure 3B** shows the linear relationship observed between $[SA]_0$ and the photo-induced rate of NO_3^- depletion. The depletion rate of NO_3^- was minimal (6.06 x 10^{-6} s^{-1}) for these droplets with $[SA]_0 = 0$ m, hence the results here indicate that CA does not induce noticeable depletion of NO_3^- and there is no nitrate depletion due to HNO_3 partitioning[37] for these relatively large (80-100 μm diameter) and viscous aqueous droplets. Measurements of [NO_3^-] with and

without 266 nm irradiation further proves that excitation of SA is necessary for reactions of NO_3^- (**Figure S3**) to proceed. It is worth noting that even under the acidic conditions of this experiment the evaporation of nitric acid (HNO_3) and change in droplet diameter were negligible during the ~30 minutes of reaction time (**Figure S4**). The photocatalytic effect of SA to the depletion of NO_3^- is evident given the fact that the depletion rates of NO_3^- are linearly related to $[SA]_0$ and the rates remain stable over the course of measurements.

The observed rates of NO_3^- depletion by SA with 266 nm irradiation are unexpectedly fast. For the droplet with [SA] = 75.0 x 10^{-3} m, ~40% of the nitrate was depleted after 23 minutes of 266 nm irradiation (**Figure 2A**) and the rate of NO_3^- depletion was 2.3 x 10^{-4} s^{-1} (**Figure 2B**). Comparing this value of NO_3^- depletion rate with the highest enhanced depletion rate (1.70 x 10^{-5} s^{-1}) by iron-organic complexes from the study by Gen *et al.*,[30] the depletion rate from our measurement is more than an order of magnitude higher although the mechanism of nitrate depletion is different. Additionally, the observed rate of depletion from this study is comparable to accelerated photolysis rates of NO_3^- in particles (10^{-4} – 10^{-5} s^{-1}).[38–40] This striking enhancement of NO_3^- depletion rate by excited-state SA without direct photolysis clearly demonstrates the effectiveness of SA as a photocatalyst for reduction of NO_3^-. A control experiment was conducted with hydrogen peroxide (H_2O_2) instead of SA, thus producing ·OH in the droplet by 266 nm photolysis of H_2O_2.[41] The result showed no significant decrease of $[NO_3^-]$ and droplet diameter during the 266 nm irradiation with H_2O_2 (**Figure S5**). These observations rule out the possibility of NO_3^- depletion by ·OH that is typically produced in photosensitized reactions.[42,43,31,44–46] The oxidation of CA was also not noticeable from **Figure S5**, given that the droplet diameter and Raman intensity ratio of ν(C=O) to ν(C-H) remained stable.[45,46] Additionally, the rate of NO_3^- depletion in droplets with varying $[NO_3^-]_0$ and fixed $[SA]_0$ in solution was also measured, and

slower depletion rates for higher $[NO_3^-]_0$ were observed (**Figure S6**). This trend may arise from the hygroscopicity of $NaNO_3$, as more NO_3^- leads to larger water content in droplets and diluting [SA] in droplets, thus decreasing the depletion rate as $[NO_3^-]_0$ increases. These thorough examinations further confirm that the reduction of NO_3^- (eq. 1 and 2) can proceed without the photolysis of NO_3^- but indirectly and efficiently promoted by the presence of excited-state SA.

In addition to the depletion of NO_3^-, the volume of the droplets with SA decreased during 266 nm irradiation as shown in **Figure 3C**. The droplets with higher [SA] showed a higher volume reduction (*VR*) which is defined as follows,

$$VR = \frac{V_f}{V_i} \qquad (4)$$

where V_i is the volume of the droplet at the start (t = 0) of 266 nm irradiation and V_f is the volume of the droplet measured at the end of the run. It is clear that the volume reduction of the droplets is caused by the photochemical reactions triggered by the excited-state SA, as NO_3^- molecules can transform into volatile compounds such as NO_2 and HONO gas. Eq. 1 is a possible pathway for nitrate reduction and the produced NO_2 (g) can partition from the droplet surface. Given that the droplets are in highly acidic conditions solely due to CA (pH ~0.6), the NO_2^- produced from eq. 2 can readily form HONO (g) (eq. 3) and escape the droplets as well.[31] Depletion of NO_3^- from the droplet is accompanied by the evaporation of water because of the hygroscopic effect of NO_3^-.[47] Therefore, the droplets with 266 nm irradiation show *VR* (**Figure 3C**) as well as a decrease in droplet mass. Stable trapping condition of a single droplet in the EDB is dependent on the mass-to-charge ratio (m/q).[48] The volume and mass determines the upper bound (~30 minutes) limit of the droplet trapping time with 266 nm irradiation as the loss of NO_3^- and water driving the reduction in droplet volume drives the droplet outside of the range of m/q required for stable trapping conditions in the EDB.

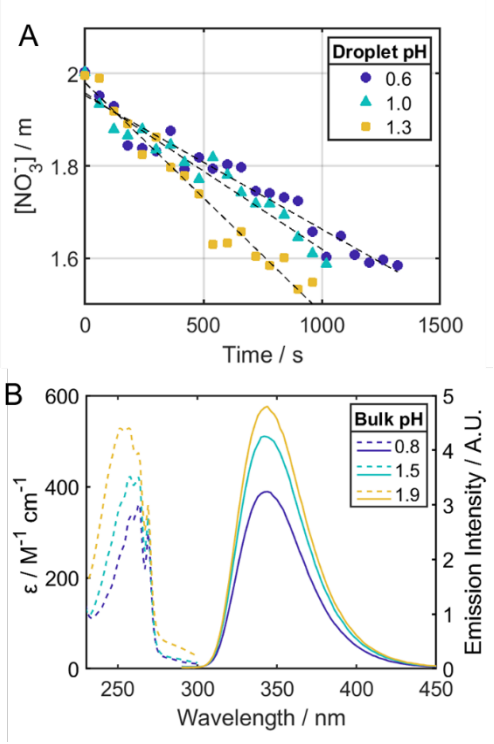

Figure 4. pH-dependence of NO_3^- depletion rate and absorption-emission properties of SA. (A) [NO_3^-] versus time at different acidic pH conditions of the droplets and fixed SA content ([SA] = 45.0 x 10^{-3} m). (B) Absorption (dashed lines) and emission (solid lines) spectra of SA in bulk aqueous solutions with varying pH.

To further support the role of excited-state SA for enhanced reactions of NO_3^-, the depletion rate and absorption-emission spectra of SA at three different acidic pH conditions (pH 0.8 – 1.9) were measured. The pH conditions of droplets were adjusted by varying CA/trisodium citrate molar ratio of the initial solutions (**Figure S7**). **Figure 4A** shows that the depletion of NO_3^- is faster for less-acidic droplets. This pH-dependence of NO_3^- depletion rate in acidic conditions can be related to the absorption and emission character of SA. In **Figure 4B**, it is clear that the molar absorptivity (ε) and emission intensity of SA rise as the pH of the solution increases from

0.6 to 1.3. It can be inferred that in less acidic conditions a higher population of excited-state SA molecules are available for NO_3^- to react, thus increasing the rate of NO_3^- depletion.

Observations of enhanced NO_3^- depletion from excited-state SA lead to an important question: what is the underlying mechanism of the photocatalytic effect of SA? We propose a triplet-triplet energy transfer (TTET) mechanism between SA and NO_3^- which is supported by absorption-emission analysis and excitation energy calculations. From **Figure 1**, it is noticeable that there is a significant energy gap between the absorption and emission spectra of SA. Comparing the energy with respect to the λ_{max} for absorption (263 nm) and emission (344 nm) yields a significant energy difference of 1.11 eV. Therefore, it is plausible that the observed emission of SA (**Figure 1**) resulting from 266 nm excitation is phosphorescence, *i.e.*, the photoexcited singlet-excited state (S_1) undergoes radiationless intersystem crossing (ISC) to the triplet-excited state (T_1) that then phosphoresces by relaxation to singlet-ground state ($T_1 \rightarrow S_0$).[49]

This argument is supported by time-dependent density functional theory (TD-DFT) calculations of the excited-state energies, as tabulated in **Table 1**. Note that both the zwitterionic (net charge 0) and protonated (net charge +1) forms of SA were included in the excited-state calculations because these two forms of SA coexist under the acidic conditions of the droplet experiment. It was shown from the calculation that the energy differences between SA (S_1) and SA (T_1) is 1.10 and 1.32 eV for protonated and zwitterionic forms of SA, respectively, (**Table 1**) in agreement with the observed 1.11 eV red-shift from the experiment. To accurately calculate the excited state energetics of SA, a vertical excitation to S_1 was assumed, while the relaxation energy from equilibrium geometry of the S_1 excited state was calculated for T_1. The polarizable continuum model (PCM) was used to include the solvation effect of water.[50] The optimized geometries for excited and ground states of both zwitterionic and protonated SA are reported in SI **Table S1**.

From the TD-DFT calculation, the excitation energy of NO_3^- shows about 0.4 eV difference between S_1 and T_1 states (**Table 1**). The calculated energy difference between the S_1 and T_1 states of NO_3^- can vary from 0.2 to 0.4 eV depending on the computational method used, [51] however, TD-DFT is chosen in this work for consistency of the energy calculations of both vertical excitation and relaxed geometries. Given that the emission of SA (T_1) (zwitterion: 3.57 eV protonated: 3.80 eV) and excitation of NO_3^- (T_1) (3.44 eV) have comparable energy values, TTET can occur between them when wavefunctions of two states overlap. To verify the TTET process in droplets, a set of experiments were performed with different chamber environments: 100% N_2 vs zero air (80% N_2 + 20% O_2). As shown in **Figure S8**, the depletion of NO_3^- was decelerated by a factor of 2 in the presence of zero air, likely due to triplet quenching by dissolved oxygen in the droplet.[52] The TTET mechanism is often referred to as photosensitization, and it is believed to contribute significantly to the overall redox chemistry of the aerosols in Earth's atmosphere.[44] The graphical description of the photosensitization process between SA and NO_3^- leading to the depletion of NO_3^- in the droplet is shown in **Figure 5**. First, SA (S_0) is excited to S_1 state by absorbing 266 nm radiation, followed by ISC from SA (S_1) to SA (T_1). Then, TTET takes place between SA (T_1) and NO_3^- (S_0), resulting in SA (S_0) and NO_3^- (T_1) according to the rule of spin conservation. Finally, NO_3^- (T_1) molecules are reduced to NO_2 (g) and HONO (g) (eq. 1 and 2), and the products evaporate from the droplet. After TTET, SA (S_0) can again absorb a 266 nm photon, serving as a photocatalyst for the photo-induced reactions of NO_3^-.

Table 1. Excited-state energies of aqueous phase SA and NO_3^- calculated using TD-DFT with 6-31+G(p,d) basis set.

	ΔE (S_1) / eV	ΔE (T_1) / eV
NO_3^-	3.87	3.44
SA (zwitterion)	4.89	3.57
SAH^+ (protonated)	4.90	3.80

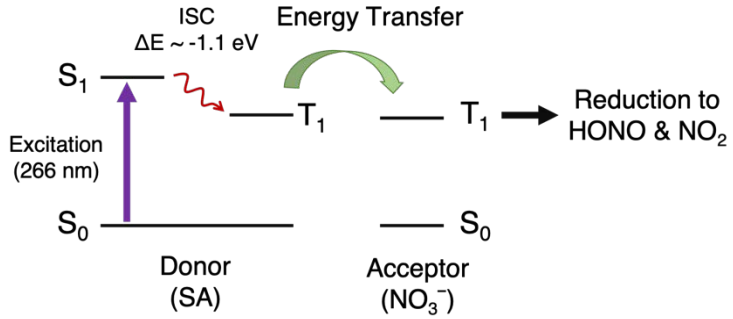

Figure 5. Energy level diagram for triplet-triplet energy transfer (TTET) between SA and NO_3^-.

It is interesting that the NO_3^- (T_1) state has been a subject of various theoretical studies, and it was suggested that the T_1 state can contribute to the effective photolysis of NO_3^-.[23,51,53] Svoboda *et al.* argued that the dissociation (reduction) of NO_3^- is more likely from the T_1 state than the S_1 state, suggesting that the singlet to triplet absorption of NO_3^- can be an important step for NO_3^- reduction.[51] However, singlet-triplet absorption of NO_3^- has not been observed experimentally, due to the dipole- and spin-forbidden nature of this transition.[23,24] Here, our result

of nitrate depletion from **Figure 3** and the proposed TTET mechanism shown in **Figure 5** can provide an important piece of scientific data toward understanding the efficient reduction of triplet-excited NO_3^-. To be specific, dissociation of NO_3^- from T_1 state can be effectively mediated through TTET rather than forbidden singlet-triplet absorption ($S_0 \rightarrow T_1$). Although the definition of the spin state of SA was not investigated by other techniques such as fluorescence lifetime measurements, the efficient photocatalytic effect of SA for NO_3^- reduction and quenching by dissolved oxygen strongly supports the role of triplet SA as a photosensitizer. The lifetime of the triplet state can be estimated to be on the order of tens of microseconds (μs) according to the literature, where similar photosensitizers were studied in the context of CDOM aquatic photochemistry.[54,55]

The result of this study unambiguously shows the reduction reactions (eq. 1 and 2) of NO_3^- are triggered by SA (T_1) without the photolysis of NO_3^-. In previous studies of photosensitized reactions of NO_3^-, one of the proposed mechanisms for enhanced reduction rate of NO_3^- involves the production of solvated electrons (e_s^-) from the UV-irradiated photosensitizers (eq. 5, *Ph*: photosensitizer) followed by the reaction between NO_3^- and e_s^- (eq. 6).[29]

$$Ph + hv \rightarrow Ph^* \rightarrow Ph^+ + e_s^- \quad (5)$$

$$NO_3^- + e_s^- \rightarrow NO_3^{2-} \quad (6)$$

However, the production of the NO_3^{2-} radical from the one-electron reduction of NO_3^- is not favored thermodynamically ($E° \approx -1.1$ V vs NHE) and the collision between two negatively charged particles may not be a frequent event in aqueous solutions due to the strong Coulombic repulsion.[56] In comparison, reaction (6) is more unfavorable than the reduction of water by e_s^- given in eq. 7 ($E° = -0.83$ V vs NHE).[57]

$$H_2O + e_s^- \rightarrow \frac{1}{2}H_2 + OH^- \quad (7)$$

Therefore, in this study, we suggest the TTET mechanism as a more plausible explanation for the depletion of NO_3^- in the presence of organic photosensitizers. Enhanced production of HONO by an energy transfer mechanism through organic chromophores can potentially contribute to the missing budget of daytime HONO production. Furthermore, this study expands our understanding of nitrate photochemistry within single aqueous droplets, an active area of research that has recently shown some additional aspects of nitrate photochemistry including the importance of the role of excited states,[32] and aqueous aerosol size,[38] as well as the impact on halogen cycling for this reaction.[58]

In conclusion, in-situ spectroscopic analysis of single levitated droplets with 266 nm laser irradiation revealed depletion of NO_3^- promoted by energy transfer from triplet excited-state SA to ground-state NO_3^-. The rate of NO_3^- depletion and volume reduction of droplets were directly dependent on the initial concentration of SA, suggesting the photocatalytic role of SA for reduction of NO_3^-. It is expected that the main products for the reactions are NO_2 and HONO, and they readily evaporate from the droplet surface, leading to the observed decrease in droplet volume. Absorption-emission spectra of SA and NO_3^- along with TD-DFT excited state energy calculations and the effect of dissolved oxygen on the NO_3^- depletion kinetics suggest that TTET occurs between the two species. Moreover, the absorption and emission character of SA with varying pH conditions are correlated with the depletion rate of NO_3^-, consistent with a larger population of SA (T_1) leading to faster NO_3^- depletion. The experimental results reported in this work provide a new mechanism for how photochemical reactions of aqueous NO_3^- can be enhanced by TTET from light-absorbing organic compounds and,[29–31] more broadly, on promoting optically forbidden transitions in a molecule facilitated by a nearby chromophore.[59]

Experimental Methods

Details of the experimental and computational methods used in this study are given in the Supporting Information (SI). The EDB was enclosed by an environmental chamber and the relative humidity (RH) in the chamber was kept constant at 80% for every measurement (**Figure S10**). The measured average powers of laser beams were ~0.075 mW (1.7×10^{-10} Einstein / s) and ~40 mW (1.8×10^{-7} Einstein / s) for 266 and 532 nm output, respectively. Both laser beams are vertically polarized in the laboratory frame. Note that the beam waist of 266 nm laser irradiation (<500 μm) is larger than the droplet diameter (~80 μm), thus not all photons with 266 nm energy interact with the droplet. The size of the droplets were estimated by MSI (**Figure S2, S9**), with the real refractive index (n) of the droplets approximated by the n values of aqueous CA and aqueous $NaNO_3$ droplets at 80% RH.[60,61] Molal (m) concentration was chosen as a unit for concentrations of solutes in the droplets because the molar ratios were converted to molal concentrations in the AIOMFAC model which is widely used for the water activity parametrization of ionic and organic mixtures.[62] TD-DFT calculations for ground and excited state energies of NO_3^- and SA were carried out using Gaussian09 software.[63]

ASSOCIATED CONTENT

Supporting Information.

The following files are available free of charge.

Materials and methods, calibration curve for determination of [NO_3^-], results of control experiments, illustration of MSI process, droplet diameters over time, adjusting droplet pH using citrate buffer, and schematic diagram of EDB with optical layout. (PDF)

AUTHOR INFORMATION

Corresponding Authors

Vicki H. Grassian*, orcid.org/0000-0001-5052-0045, Email: vhgrassian@ucsd.edu

Department of Chemistry and Biochemistry, University of California San Diego, 9500 Gilman Drive, La Jolla, California, 92093-0340, United States

Robert E. Continetti*, orcid.org/0000-0002-0685-4459, Email: rcontinetti@ucsd.edu

Department of Chemistry and Biochemistry, University of California San Diego, 9500 Gilman Drive, La Jolla, California, 92093-0340, United States

Authors

Pyeongeun Kim, orcid.org/0000-0002-4718-4770

Department of Chemistry and Biochemistry, University of California San Diego, 9500 Gilman Drive, La Jolla, California, 92093-0340, United States

Now at Chemical Sciences Division, Lawrence Berkeley National Laboratory, 1 Cyclotron Road, Berkeley, California, 94720, United States

Christian Boothby

Department of Chemistry and Biochemistry, University of California San Diego, 9500 Gilman Drive, La Jolla, California, 92093-0340, United States

Notes

The authors declare no competing financial interests.

ACKNOWLEDGMENT

We thank Satavisa Jana and Prof. Judy Kim for their help with the UV-Vis spectrometer and fluorometer. P.K. thanks Stephanie Mora-Garcia and Kyle Angle for helpful discussions about nitrate photochemistry. This work was supported by the NSF through the NSF Center for Aerosol Impacts on Chemistry of the Environment (CAICE), CHE-1801971. C.B. was supported by the AFOSR (MURI-22 FA9550-22-1-0199).

REFERENCES

(1) McCormick, R. A.; Ludwig, J. H. Climate Modification by Atmospheric Aerosols. *Science* **1967**, *156* (3780), 1358 LP – 1359.

(2) Field, C. B.; Barros, V. R. *Climate Change 2014–Impacts, Adaptation and Vulnerability: Regional Aspects*; Cambridge University Press, 2014.

(3) Mauderly, J. L.; Chow, J. C. Health Effects of Organic Aerosols. *Inhalation toxicology* **2008**, *20* (3), 257–288.

(4) Wang, C. C.; Prather, K. A.; Sznitman, J.; Jimenez, J. L.; Lakdawala, S. S.; Tufekci, Z.; Marr, L. C. Airborne Transmission of Respiratory Viruses. *Science* **2021**, *373* (6558).

(5) Grassian, V. H. Heterogeneous Uptake and Reaction of Nitrogen Oxides and Volatile Organic Compounds on the Surface of Atmospheric Particles Including Oxides, Carbonates, Soot and Mineral Dust: Implications for the Chemical Balance of the Troposphere. *International Reviews in Physical Chemistry* **2001**, *20* (3), 467–548.

(6) Shrivastava, M.; Lou, S.; Zelenyuk, A.; Easter, R. C.; Corley, R. A.; Thrall, B. D.; Rasch, P. J.; Fast, J. D.; Simonich, S. L. M.; Shen, H.; Tao, S. Global Long-Range Transport and Lung

Cancer Risk from Polycyclic Aromatic Hydrocarbons Shielded by Coatings of Organic Aerosol. *Proceedings of the National Academy of Sciences of the United States of America* **2017**, *114* (6), 1246–1251.

(7) Zeng, M.; Wilson, K. R. Efficient Coupling of Reaction Pathways of Criegee Intermediates and Free Radicals in the Heterogeneous Ozonolysis of Alkenes. *Journal of Physical Chemistry Letters* **2020**, *11* (16), 6580–6585.

(8) Dalton, A. B.; Nizkorodov, S. A. Photochemical Degradation of 4-Nitrocatechol and 2,4-Dinitrophenol in a Sugar-Glass Secondary Organic Aerosol Surrogate. *Environmental Science and Technology* **2021**, *55* (21), 14586–14594.

(9) Kim, P.; Continetti, R. E. Accelerated Keto-Enol Tautomerization Kinetics of Malonic Acid in Aqueous Droplets. *ACS Earth and Space Chemistry* **2021**, *5* (9), 2212–2222.

(10) Zafiriou, O. C.; True, M. B. Nitrate Photolysis in Seawater by Sunlight. *Marine Chemistry* **1979**, *8* (1), 33–42.

(11) Li, J.; Gao, W.; Cao, L.; Xiao, Y.; Zhang, Y.; Zhao, S.; Liu, Z.; Liu, Z.; Tang, G.; Ji, D.; Hu, B.; Song, T.; He, L.; Hu, M.; Wang, Y. Significant Changes in Autumn and Winter Aerosol Composition and Sources in Beijing from 2012 to 2018: Effects of Clean Air Actions. *Environmental Pollution* **2021**, *268*, 115855.

(12) Vero, S. E.; Basu, N. B.; Van Meter, K.; Richards, K. G.; Mellander, P.-E.; Healy, M. G.; Fenton, O. Review: The Environmental Status and Implications of the Nitrate Time Lag in Europe and North America. *Hydrogeol J* **2018**, *26* (1), 7–22.

(13) Mack, J.; Bolton, J. R. Photochemistry of Nitrite and Nitrate in Aqueous Solution: A Review. *Journal of Photochemistry and Photobiology A: Chemistry* **1999**, *128* (1–3), 1–13.

(14) Comes, F. J. Recycling in the Earth's Atmosphere: The OH Radical—Its Importance for the Chemistry of the Atmosphere and the Determination of Its Concentration. *Angewandte Chemie International Edition in English* **1994**, *33* (18), 1816–1826.

(15) Arakaki, T.; Miyake, T.; Hirakawa, T.; Sakugawa, H. pH Dependent Photoformation of Hydroxyl Radical and Absorbance of Aqueous-Phase N(III) (HNO2 and NO2-). *Environmental Science and Technology* **1999**, *33* (15), 2561–2565.

(16) Han, C.; Yang, W.; Wu, Q.; Yang, H.; Xue, X. Heterogeneous Photochemical Conversion of NO2 to HONO on the Humic Acid Surface under Simulated Sunlight. *Environmental Science and Technology* **2016**, *50* (10), 5017–5023.

(17) Gen, M.; Zhang, R.; Huang, D. D.; Li, Y.; Chan, C. K. Heterogeneous Oxidation of SO_2 in Sulfate Production during Nitrate Photolysis at 300 Nm: Effect of pH, Relative Humidity, Irradiation Intensity, and the Presence of Organic Compounds. *Environ. Sci. Technol.* **2019**, *53* (15), 8757–8766.

(18) Zhang, R.; Gen, M.; Huang, D.; Li, Y.; Chan, C. K. Enhanced Sulfate Production by Nitrate Photolysis in the Presence of Halide Ions in Atmospheric Particles. *Environ. Sci. Technol.* **2020**, *54* (7), 3831–3839.

(19) Zhang, R.; Gen, M.; Liang, Z.; Li, Y. J.; Chan, C. K. Photochemical Reactions of Glyoxal during Particulate Ammonium Nitrate Photolysis: Brown Carbon Formation, Enhanced Glyoxal Decay, and Organic Phase Formation. *Environ. Sci. Technol.* **2022**, *56* (3), 1605–1614.

(20) Mabato, B. R. G.; Lyu, Y.; Ji, Y.; Li, Y. J.; Huang, D. D.; Li, X.; Nah, T.; Lam, C. H.; Chan, C. K. Aqueous Secondary Organic Aerosol Formation from the Direct Photosensitized

Oxidation of Vanillin in the Absence and Presence of Ammonium Nitrate. *Atmos. Chem. Phys.* **2022**, *22* (1), 273–293.

(21) Mabato, B. R. G.; Li, Y. J.; Huang, D. D.; Wang, Y.; Chan, C. K. Comparison of Aqueous Secondary Organic Aerosol (aqSOA) Product Distributions from Guaiacol Oxidation by Non-Phenolic and Phenolic Methoxybenzaldehydes as Photosensitizers in the Absence and Presence of Ammonium Nitrate. *Atmos. Chem. Phys.* **2023**, *23* (4), 2859–2875.

(22) Goldstein, S.; Rabani, J. Mechanism of Nitrite Formation by Nitrate Photolysis in Aqueous Solutions: The Role of Peroxynitrite, Nitrogen Dioxide, and Hydroxyl Radical. *Journal of the American Chemical Society* **2007**, *129* (34), 10597–10601.

(23) Svoboda, O.; Kubelová, L.; Slavíček, P. Enabling Forbidden Processes: Quantum and Solvation Enhancement of Nitrate Anion UV Absorption. *Journal of Physical Chemistry A* **2013**, *117* (48), 12868–12877.

(24) Marcotte, G.; Marchand, P.; Pronovost, S.; Ayotte, P.; Laffon, C.; Parent, P. Surface-Enhanced Nitrate Photolysis on Ice. *Journal of Physical Chemistry A* **2015**, *119* (10), 1996–2005.

(25) Scharko, N. K.; Berke, A. E.; Raff, J. D. Release of Nitrous Acid and Nitrogen Dioxide from Nitrate Photolysis in Acidic Aqueous Solutions. *Environmental Science and Technology* **2014**, *48* (20), 11991–12001.

(26) Couzo, E.; Lefer, B.; Stutz, J.; Yarwood, G.; Karamchandani, P.; Henderson, B.; Vizuete, W. Impacts of Heterogeneous HONO Formation on Radical Sources and Ozone Chemistry in Houston, Texas. *Atmospheric Environment* **2014**, *112*, 344–355.

(27) Lee, J. D.; Whalley, L. K.; Heard, D. E.; Stone, D.; Dunmore, R. E.; Hamilton, J. F.; Young, D. E.; Allan, J. D.; Laufs, S.; Kleffmann, J. Detailed Budget Analysis of HONO in Central

London Reveals a Missing Daytime Source. *Atmospheric Chemistry and Physics* **2016**, *16* (5), 2747–2764.

(28) Ye, C.; Zhang, N.; Gao, H.; Zhou, X. Photolysis of Particulate Nitrate as a Source of HONO and NOx. *Environmental Science and Technology* **2017**, *51* (12), 6849–6856.

(29) Wang, Y.; Huang, D. D.; Huang, W.; Liu, B.; Chen, Q.; Huang, R.; Gen, M.; Mabato, B. R. G.; Chan, C. K.; Li, X.; Hao, T.; Tan, Y.; Hoi, K. I.; Mok, K. M.; Li, Y. J. Enhanced Nitrite Production from the Aqueous Photolysis of Nitrate in the Presence of Vanillic Acid and Implications for the Roles of Light-Absorbing Organics. *Environmental Science and Technology* **2021**, *55* (23), 15694–15704.

(30) Gen, M.; Zhang, R.; Chan, C. K. Nitrite/Nitrous Acid Generation from the Reaction of Nitrate and Fe(II) Promoted by Photolysis of Iron-Organic Complexes. *Environmental Science and Technology* **2021**, *55* (23), 15715–15723.

(31) Mora Garcia, S. L.; Pandit, S.; Navea, J. G.; Grassian, V. H. Nitrous Acid (HONO) Formation from the Irradiation of Aqueous Nitrate Solutions in the Presence of Marine Chromophoric Dissolved Organic Matter: Comparison to Other Organic Photosensitizers. *ACS Earth and Space Chemistry* **2021**, *5* (11), 3056–3064.

(32) Jiang, H.; Bao, F.; Wang, J.; Chen, J.; Zhu, Y.; Huang, D.; Chen, C.; Zhao, J. Direct Formation of Electronic Excited NO_2 Contributes to the High Yield of HONO during Photosensitized Renoxification. *Environ. Sci. Technol.* **2023**, acs.est.3c01342.

(33) Nadler, K. A.; Kim, P.; Huang, D. L.; Xiong, W.; Continetti, R. E. Water Diffusion Measurements of Single Charged Aerosols Using H2O/D2O Isotope Exchange and Raman Spectroscopy in an Electrodynamic Balance. *Physical Chemistry Chemical Physics* **2019**, *21* (27), 15062–15071.

(34) Kim, P.; Xiong, W.; Continetti, R. E. Evolution of Hydrogen-Bond Interactions within Single Levitated Metastable Aerosols Studied by in Situ Raman Spectroscopy. *Journal of Physical Chemistry B* **2020**, *124* (42), 9385–9395.

(35) Yang, X.; Zhang, Y.; Wang, L.; Cao, L.; Li, K.; Hursthouse, A. Preparation of a Thermally Modified Diatomite and a Removal Mechanism for 1-Naphthol from Solution. *Water (Switzerland)* **2017**, *9* (9), 1–15.

(36) Pandit, S.; Mora Garcia, S. L.; Grassian, V. H. HONO Production from Gypsum Surfaces Following Exposure to NO2and HNO3: Roles of Relative Humidity and Light Source. *Environmental Science and Technology* **2021**, *55* (14), 9761–9772.

(37) Angle, K. J.; Grassian, V. H. Direct Quantification of Changes in pH within Single Levitated Microdroplets and the Kinetics of Nitrate and Chloride Depletion. *Chem. Sci.* **2023**, *14* (23), 6259–6268.

(38) Gen, M.; Liang, Z.; Zhang, R.; Go Mabato, B. R.; Chan, C. K. Particulate Nitrate Photolysis in the Atmosphere. *Environ. Sci.: Atmos.* **2022**, *2* (2), 111–127.

(39) Bao, F.; Li, M.; Zhang, Y.; Chen, C.; Zhao, J. Photochemical Aging of Beijing Urban PM $_{2.5}$: HONO Production. *Environ. Sci. Technol.* **2018**, *52* (11), 6309–6316.

(40) Romer, P. S.; Wooldridge, P. J.; Crounse, J. D.; Kim, M. J.; Wennberg, P. O.; Dibb, J. E.; Scheuer, E.; Blake, D. R.; Meinardi, S.; Brosius, A. L.; Thames, A. B.; Miller, D. O.; Brune, W. H.; Hall, S. R.; Ryerson, T. B.; Cohen, R. C. Constraints on Aerosol Nitrate Photolysis as a Potential Source of HONO and NO $_x$. *Environ. Sci. Technol.* **2018**, *52* (23), 13738–13746.

(41) Maksyutenko, P.; Radi, P. P.; Kozlov, D. N.; Kouzov, A. P. Polarization- and Time-Resolved DFWM Spectroscopy of the $A\,^2\Sigma^+ - X\,^2\Pi$ (0,0) Band Transitions of Nascent OH Radicals

Generated by 266 Nm Laser Photolysis of H_2O_2: Polarization- and Time-Resolved DFWM. *J. Raman Spectrosc.* **2013**, *44* (10), 1349–1355.

(42) Nikitenko, S. I.; Venault, L.; Moisy, Ph. Scavenging of OH Radicals Produced from H2O Sonolysis with Nitrate Ions. *Ultrasonics Sonochemistry* **2004**, *11* (3–4), 139–142.

(43) Goldstein, S.; Aschengrau, D.; Diamant, Y.; Rabani, J. Photolysis of Aqueous H2O2: Quantum Yield and Applications for Polychromatic UV Actinometry in Photoreactors. *Environmental Science and Technology* **2007**, *41* (21), 7486–7490.

(44) Martins-Costa, M. T. C.; Anglada, J. M.; Francisco, J. S.; Ruiz-López, M. F. Photosensitization Mechanisms at the Air-Water Interface of Aqueous Aerosols. *Chemical Science* **2022**, *13* (9), 2624–2631.

(45) Corral Arroyo, P.; Bartels-Rausch, T.; Alpert, P. A.; Dumas, S.; Perrier, S.; George, C.; Ammann, M. Particle-Phase Photosensitized Radical Production and Aerosol Aging. *Environ. Sci. Technol.* **2018**, *52* (14), 7680–7688.

(46) Corral Arroyo, P.; Aellig, R.; Alpert, P. A.; Volkamer, R.; Ammann, M. Halogen Activation and Radical Cycling Initiated by Imidazole-2-Carboxaldehyde Photochemistry. *Atmos. Chem. Phys.* **2019**, *19* (16), 10817–10828.

(47) Jing, B.; Wang, Z.; Tan, F.; Guo, Y.; Tong, S.; Wang, W.; Zhang, Y.; Ge, M. Hygroscopic Behavior of Atmospheric Aerosols Containing Nitrate Salts and Water-Soluble Organic Acids. *Atmospheric Chemistry and Physics* **2018**, *18* (7), 5115–5127.

(48) Trevitt, A. J.; Wearne, P. J.; Bieske, E. J. Calibration of a Quadrupole Ion Trap for Particle Mass Spectrometry. *International Journal of Mass Spectrometry* **2007**, *262* (3), 241–246.

(49) Lysenko, G. M.; Kislyak, G. M. On Photoluminescence Reabsorption in Organic Phosphors. *Journal of Applied Spectroscopy* **1967**, *7* (3), 272–275.

(50) Mennucci, B. Polarizable Continuum Model. *WIREs Comput Mol Sci* **2012**, *2* (3), 386–404.

(51) Svoboda, O.; Slavíček, P. Is Nitrate Anion Photodissociation Mediated by Singlet-Triplet Absorption? *Journal of Physical Chemistry Letters* **2014**, *5* (11), 1958–1962.

(52) Gong, C.; Yuan, X.; Xing, D.; Zhang, D.; Martins-Costa, M. T. C.; Anglada, J. M.; Ruiz-López, M. F.; Francisco, J. S.; Zhang, X. Fast Sulfate Formation Initiated by the Spin-Forbidden Excitation of SO_2 at the Air–Water Interface. *J. Am. Chem. Soc.* **2022**, *144* (48), 22302–22308.

(53) Peterson, K. A.; Li, Y.; Francisco, J. S.; Zou, P.; Webster, C. E.; Pérez, L. M.; Hall, M. B.; North, S. W. The Role of Triplet States in the Long Wavelength Absorption Region of Bromine Nitrate. *Journal of Chemical Physics* **2003**, *119* (15), 7864–7870.

(54) Wenk, J.; Eustis, S. N.; McNeill, K.; Canonica, S. Quenching of Excited Triplet States by Dissolved Natural Organic Matter. *Environ. Sci. Technol.* **2013**, *47* (22), 12802–12810.

(55) Schmitt, M.; Erickson, P. R.; McNeill, K. Triplet-State Dissolved Organic Matter Quantum Yields and Lifetimes from Direct Observation of Aromatic Amine Oxidation. *Environ. Sci. Technol.* **2017**, *51* (22), 13151–13160.

(56) Cook, A. R.; Dimitrijevic, N.; Dreyfus, B. W.; Meisel, D.; Curtiss, L. A.; Camaioni, D. M. Reducing Radicals in Nitrate Solutions. The NO32- System Revisited. *Journal of Physical Chemistry A* **2001**, *105* (14), 3658–3666.

(57) Lide, D. R. *CRC Handbook of Chemistry and Physics. 79th Ed.*; CRC Press Inc.: Boca Raton, FL, 1998.

(58) Dalton, E. Z.; Hoffmann, E. H.; Schaefer, T.; Tilgner, A.; Herrmann, H.; Raff, J. D. Daytime Atmospheric Halogen Cycling through Aqueous-Phase Oxygen Atom Chemistry. *J. Am. Chem. Soc.* **2023**, *145* (29), 15652–15657.

(59) Takenaka, N.; Daimon, T.; Ueda, A.; Sato, K.; Kitano, M.; Bandow, H.; Maeda, Y. Fast Oxidation Reaction of Nitrite by Dissolved Oxygen in the Freezing Process in the Tropospheric Aqueous Phase. *Journal of Atmospheric Chemistry* **1998**, *29*, 135–150.

(60) Mason, B. J.; King, S. J.; Miles, R. E. H.; Manfred, K. M.; Rickards, A. M. J.; Kim, J.; Reid, J. P.; Orr-Ewing, A. J. Comparison of the Accuracy of Aerosol Refractive Index Measurements from Single Particle and Ensemble Techniques. *Journal of Physical Chemistry A* **2012**, *116* (33), 8547–8556.

(61) Lienhard, D. M.; Bones, D. L.; Zuend, A.; Krieger, U. K.; Reid, J. P.; Peter, T. Measurements of Thermodynamic and Optical Properties of Selected Aqueous Organic and Organic-Inorganic Mixtures of Atmospheric Relevance. *Journal of Physical Chemistry A* **2012**, *116* (40), 9954–9968.

(62) Zuend, A.; Marcolli, C.; Booth, A. M.; Lienhard, D. M.; Soonsin, V.; Krieger, U. K.; Topping, D. O.; McFiggans, G.; Peter, T.; Seinfeld, J. H. New and Extended Parameterization of the Thermodynamic Model AIOMFAC: Calculation of Activity Coefficients for Organic-Inorganic Mixtures Containing Carboxyl, Hydroxyl, Carbonyl, Ether, Ester, Alkenyl, Alkyl, and Aromatic Functional Groups. *Atmospheric Chemistry and Physics* **2011**, *11* (17), 9155–9206.

(63) Frisch, M. J.; Trucks, G. W.; Schlegel, H. B.; Scuseria, G. E.; Robb, M. A.; Cheeseman, J. R.; Scalmani, G.; Barone, V.; Petersson, G. A.; Nakatsuji, H.; Li, X.; Caricato, M.; Marenich, A. V.; Bloino, J.; Janesko, B. G.; Gomperts, R.; Mennucci, B.; Hratch, D. J. Gaussian 09, Revision A.02. Gaussian, Inc.: Wallingford CT 2016.